Semi-Lagrangian Solutions to the Inviscid Burgers Equation

HUNG-CHI KUO

Naval Environmental Prediction Research Facility, Monterey, California

R. T. WILLIAMS

Naval Postgraduate School, Monterey, California

(Manuscript received 30 June 1989, in final form 4 December 1989)

ABSTRACT

We explore the use of semi-Lagrangian methods in a situation where the spatial scale of the flow collapses to zero during the time integration. The inviscid Burgers equation is used as the test model because it is the simplest equation that allows scale collapse (shock formation), and because it has analytic solutions. It is shown that despite the variable manner in which the gradient of the wind field approaches infinity in the neighborhood of the shock, the semi-Lagrangian method allows the error to be localized near the steep slope region. Comparisons with second-order finite difference and tau methods are provided. Moreover, the semi-Lagrangian method gives accurate results even with larger time steps (Courant number greater than 2 or 4) than are possible with the Eulerian methods. The semi-Lagrangian method, along with other recently developed numerical methods, is useful in simulating the development of steep gradients or near discontinuities in a numerical model. Some applications of the semi-Lagrangian method are discussed.

1. Introduction

The need for higher resolution numerical models motivates the development of more efficient time integration schemes. A good example is the semi-implicit time integration used by Robert et al. (1972). With the semi-implicit scheme it is possible to run a primitive equation model four to six times faster than with the other frequently used integration schemes. Using concepts similar to those developed by Wiin-Nielsen (1959) and Sawyer (1963), Robert (1981) proposed combining the semi-implicit integration scheme with a semi-Lagrangian treatment of the advection terms in a barotropic model. Robert et al. (1985) extended the scheme to a multilevel model. They found that the time step could be increased by a further factor of 6 over that of an Eulerian semi-implicit scheme. Meanwhile, Bates and McDonald (1982) and Bates (1984) have shown that the semi-Lagrangian treatment of advection can also be coupled with a split explicit or alternating implicit treatment of the linear terms. McDonald (1986) and Temperton and Staniforth (1987) discussed the efficient two-time-level semi-Lagrangian methods. Staniforth and Temperton (1986) have demonstrated that the semi-Lagrangian technique with large time steps can produce excellent forecasts from synoptic scale fields as verified against high resolution Eulerian forecasts. Tanguay et al. (1989) present a 48-hour forecast from a three-dimensional semi-Lagrangian model with a time step three times larger than for an Eulerian model. Comparable results are obtained while more than halving the CPU time of the Eulerian control. In addition, Pudykiewicz and Staniforth (1984) analyzed the semi-Lagrangian approximation to the advection equation with idealized initial data and they showed that the scheme has exceptional dispersive properties. Recently, Williamson and Rasch (1989) used shape-preserving interpolation schemes in the semi-Lagrangian method to maintain the local monotonicity of the moisture fields. They applied the shape-preserving semi-Lagrangian method to the moisture advection equation in the NCAR GCM and in the NMC global model and obtained good results. Cote and Staniforth (1988) doubled the efficiency of their two-time-level semi-implicit semi-Lagrangian global spectral model by using a smaller computational Gaussian grid than the usual one, without incurring the significant loss of accuracy that is observed for the corresponding Eulerian spectral model in analogous circumstances. In these studies the spatial scales of flows did not change appreciably during the forecast period. In this paper we show that the semi-Lagrangian schemes with larger time steps perform well even when the scale collapses to zero during the integration.

There are many important phenomena in the atmosphere that are associated with sharp gradients. Hoskins and Bretherton (1972) and Williams (1967,

Corresponding author address: Dr. R. T. Williams, Code 63WU, Naval Postgraduate School, Monterey, CA 93943.

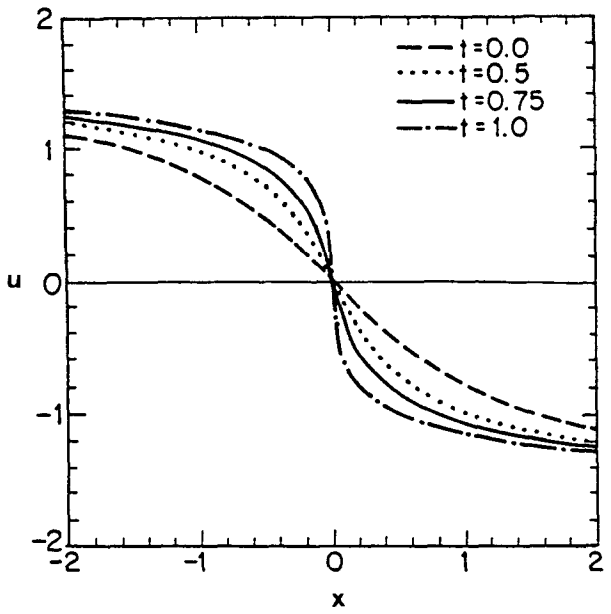

FIG. 1 The analytical solution of the inviscid Burgers equation at $t = 0.0$, $t = 0.5$, $t = 0.75$, and $t = 1.0$ with $\bar{u} = 0.0$.

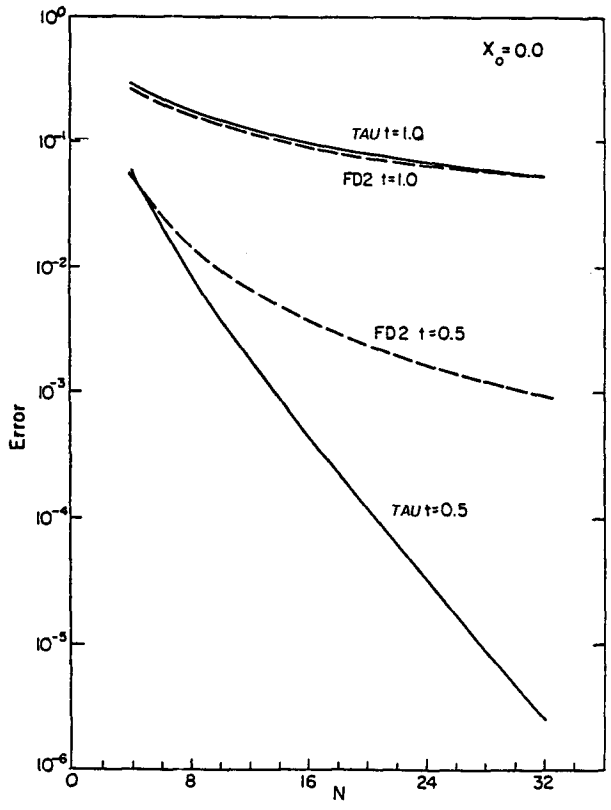

FIG. 2. The root mean square error in the numerical solutions of the inviscid Burgers equation as a function of the number of grid points (modes) N for the Chebyshev-tau (TAU) and the second-order finite difference (FD2) methods at $t = 0.5$ and $t = 1.0$ (scale-collapse time). The scale collapse position is at $x = 0.0$ and $\bar{u} = 0$.

1972) have studied frontogenesis under the combined actions of geostrophic and ageostrophic motion. They have shown that discontinuous fronts can form within a reasonable period of time if no turbulent diffusion is present. This period can be of the order of 24 hours depending on the initial conditions. Williams and Kurth (1976) examined the formation of discontinuities from unbalanced initial conditions. They determined criteria for the formation of those discontinuities that are analogous to hydraulic jumps in a one-layer homogeneous fluid. Recent observations by Shapiro et al. (1985) give evidence for the cross-front scale-collapse of nonprecipitating cold-frontal zones to hori-

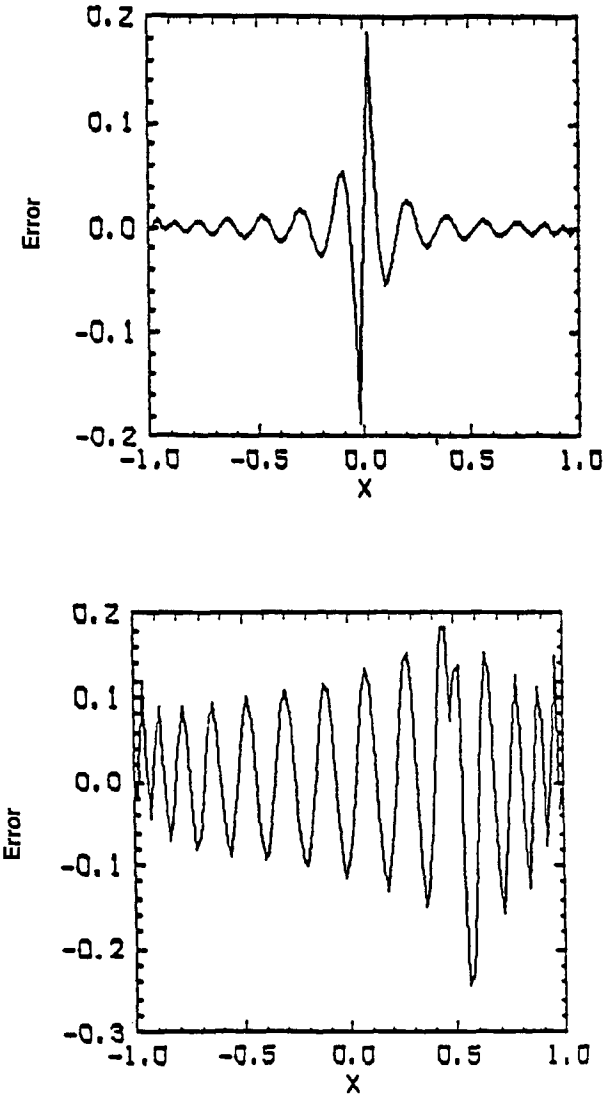

FIG. 3. The difference between the exact and the numerical solution in the computational domain at the scale-collapse time for Chebyshev-tau method with $\bar{u} = 0$. The upper picture is for the case where the scale collapse occurs at a collocation point while the lower picture is for a case where the scale collapse does not occur at a collocation point.

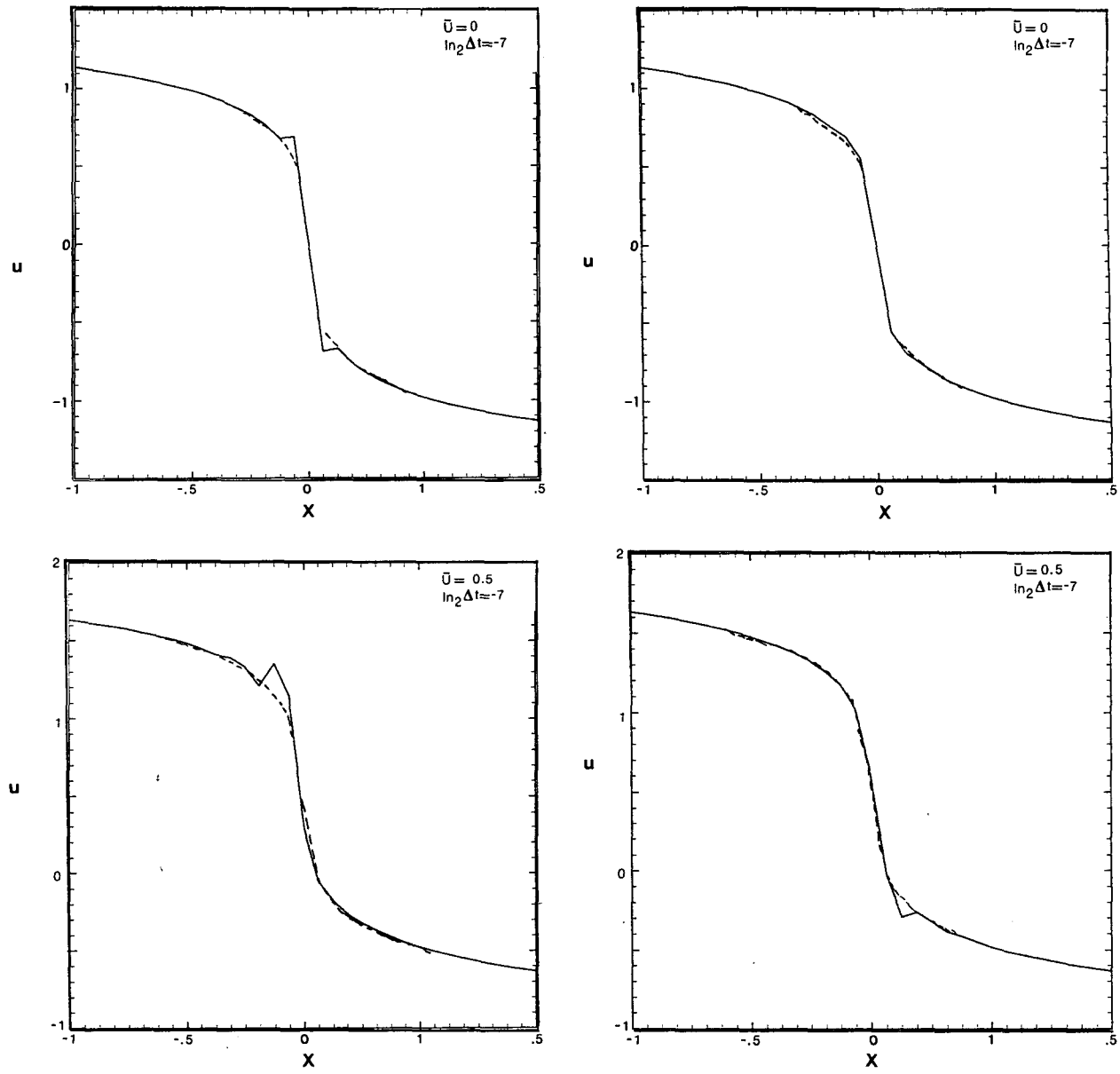

FIG. 4. The analytical and second-order finite difference solutions at the time of scale collapse with $N = 32$ and various $\bar{u}$. The dashed curves are the analytical solutions. The methods and the $\bar{u}$ are as follows: (a) FD2, $\bar{u} = 0.0$; (b) FD2C, $\bar{u} = 0.0$; (c) FD2, $\bar{u} = 0.5$; (d) FD2C, $\bar{u} = 0.5$; (e) FD2, $\bar{u} = 1.0$; (f) FD2C, $\bar{u} = 1.0$. The time step used in the calculation is 0.0078125 ($\ln_2 \Delta t = -7$).

zontal scales of 1 km or less. The leading edges of these fronts possess the characteristic structure of density current flows: an elevated hydraulic head followed by a turbulent wake. The relationship between frontal deformation, vertical circulation, and surface boundary-layer processes in frontal scale collapse and the formation of hydraulic heads remains to be studied by observational and modeling efforts.

In addition to the development of near discontinuities in frontal zones, the evolution of potential-vorticity anomalies on isentropic surfaces also involves sharp gradients. The usefulness of potential vorticity on isentropic surfaces with dynamical balance relationships (which leads to the invertability principle) in providing insight into atmospheric dynamics has been well recognized (Hoskins et al. 1985). Aside from the numerical difficulty in developing the fast elliptical solvers for the invertability principle, the treatment of the intersections of isentropic surfaces with the earth's surface can pose a challenge for numerical modelers. Following the early work of Bretherton (1966), Hoskins et al. (1985) argued that at such intersections the

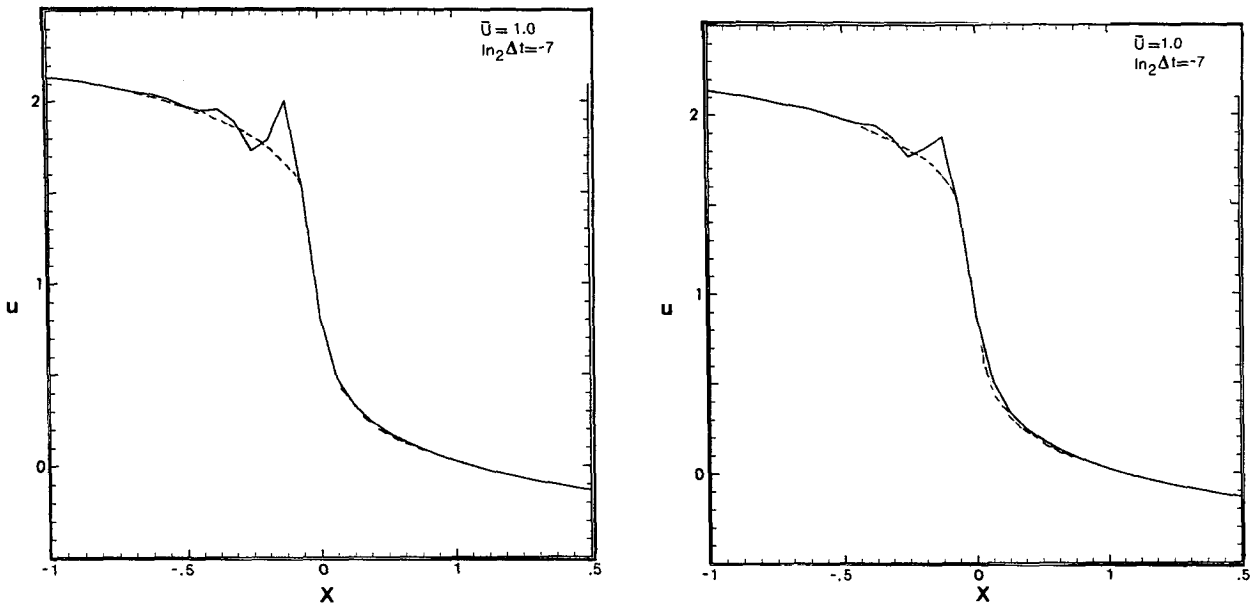

FIG. 4. (*Continued*)

isentropic surface runs just under the earth's surface with a pressure equal to the surface pressure. At any horizontal position where two distinct isentropic surfaces run just under the earth's surface, there is no mass trapped between them. Numerically, this would lead to infinite potential vorticity or zero potential pseudodensity (inverse of potential vorticity). In the prognostic equation we then need to predict the evolution of the entire potential pseudodensity (including this zero potential pseudodensity region). This implies that we must cope with sharp gradients of potential pseudodensity and guarantee the positive definiteness of potential pseudodensity.

The physical processes discussed above have implications for the computational methods used in numerical modeling. One requirement of a computational method for such scale-collapse phenomena would seem to be an ability to accurately represent a very sharp gradient in the computational domain. In addition, any numerical dispersion error due to a presence of a shock should not contaminate the smooth solution away from the shock. The problem with post-shock oscillations has lead to the development of many powerful finite difference schemes such as artificial-viscosity, self-adjusted hybrid schemes, flux-corrected transport schemes, piece-parabolic-method, and front tracking procedures. A review of these techniques can be found in Woodward and Colella (1984). In addition to the above methods, Smolarkiewicz (1984) proposed a very cost effective positive definite advection scheme with small implicit diffusion. Recently, Arakawa (personal communication) proposed a generalization of Takacs' (1985) third-order finite difference scheme that has very small dissipation and computational dispersion and that guarantees positive definiteness. In this paper, we will use the inviscid Burgers equation to illustrate the usefulness of the semi-Lagrangian method in the scale-collapse situation. The Burgers equation is used because of the shock formation in most cases and the existence of analytical solutions. Discussions of the shock solutions to Burgers equation can be found in many classical texts such as Whitham (1974). The inviscid Burgers equation and analytic solutions are given in section 2. Also presented in section 2 are the computational solutions from the tau spectral method and second-order finite difference method. The semi-Lagrangian discretization and the semi-Lagrangian solutions are given in section 3. Section 4 contains concluding remarks.

2. Model-problem and Eulerian solutions

We consider the inviscid Burgers equation

$$\frac{\partial u}{\partial t} + u\frac{\partial u}{\partial x} = 0 \tag{1}$$

on the infinite domain with the initial condition

$$u(x, 0) = f(x) = \bar{u} - \tan^{-1}(x - x_0). \tag{2}$$

The general solution to (1) is

$$u(x, t) = f(x - u(x, t)t).$$

The analytical solution for initial condition (2) is

$$u = \bar{u} - \tan^{-1}(x - ut - x_0). \tag{3}$$

To determine the time of scale-collapse differentiate (3) with respect to x which gives

$$\frac{\partial u}{\partial x} = -\frac{1 - t\dfrac{\partial u}{\partial x}}{1 + (x - x_0 - ut)^2}.$$

At $x = x_0 + \bar{u}t$, $u = \bar{u}$ so that we obtain

$$\left(\frac{\partial u}{\partial x}\right)_{x=x_0+\bar{u}t} = -\left(1 - t\left(\frac{\partial u}{\partial x}\right)_{x=x_0+\bar{u}t}\right), \quad (4)$$

which leads to

$$\left(\frac{\partial u}{\partial x}\right)_{x=x_0+\bar{u}t} = \frac{1}{t-1} \to -\infty \quad \text{as} \quad t \to 1. \quad (5)$$

Physically, the above problem gives scale-collapse formation with mean background advection at speed $\bar{u}$. The scale-collapse (shock formation) time is 1.0 with the position of scale collapse at $x_0 + \bar{u}$. Given the specified parameters $\bar{u}$ and x_0, the analytical solution to the inviscid Burgers equation with (2) as initial condition at any x and t can be obtained numerically to desired accuracy by fixed point iteration on (3). Since t varies continuously from 0 to 1, the method of continuation will speed up convergence to the iteration if we use the analytical solution computed from the previous time as the initial guess for the next time. Figure 1 shows the analytical solution of the inviscid Burgers equation at $t = 0.0$, $t = 0.5$, $t = 0.75$ and $t = 1.0$ with $x_0 = 0$ and $\bar{u} = 0$.

Once the analytical solution is established we consider the problem with the same initial condition on the finite domain $[-1, +1]$. The second-order centered difference and Chebyshev-tau methods then are used to solve the problem with the boundary conditions provided by the analtyical solution. A detailed description of the Chebyshev-tau method can be found in Gottlieb and Orszag (1977). Two types of second-order finite difference are used here. Specifically, we consider the second-order centered difference (FD2) scheme

$$\frac{du_j}{dt} + u_j \frac{u_{j+1} - u_{j-1}}{2\Delta x} = 0,$$

and the energy $(u^2/2)$ conserving second-order centered difference (FD2C) scheme

$$\frac{du_j}{dt} + \frac{(u_{j+1} + u_j + u_{j-1})(u_{j+1} - u_{j-1})}{6\Delta x} = 0. \quad (6)$$

Here u_j denotes values at the grid points x_j. The second-order Runge–Kutta time integration scheme is used here, with the time step chosen to be very small so that the errors in the computation are dominated by spatial discretization errors.

The corresponding root mean square error is shown in Fig. 2 as a function of the number of grid points N for $t = 0.5$ and $t = 1.0$ (shock formation or scale-collapse time) with $\bar{u} = 0$. The tau method is much better than the second-order finite difference method at $t = 0.5$, but both methods yield similar results at the time of scale collapse. The tau method converges exponentially to the analytical solution at $t = 0.5$ and converges algebraically to the analytical solution at $t = 1.0$. The different convergence properties for the tau spectral method are due to the fact that the smoothness of the analytical solution changes as the scale collapse occurs. The second-order finite difference method has algebraic convergence at both times. The errors (the difference between the exact and the numerical solution) as a function of x for the tau spectral method with $N = 32$ at the scale-collapse time $t = 1.0$ are presented in Fig. 3. The upper picture in Fig. 3 is for the case where the scale collapse occurs at a collocation point while the lower picture is for a case where the scale collapse does not occur at a collocation point. The root mean square error in the lower picture is about three times larger than the error in the upper picture. In both cases we observe large oscillatory errors throughout the computational domain.

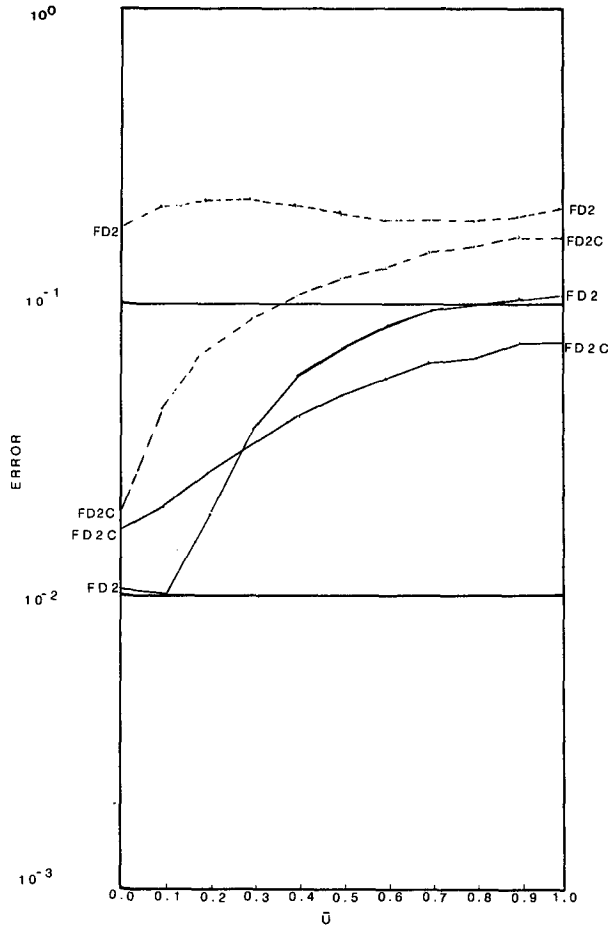

FIG. 5. The root mean square error in FD2 and FD2C schemes as a function $\bar{u}$ for $N = 32$ and $\Delta t = 0.0078125$ ($\ln_2 \Delta t = -7$) at the time of scale collapse. The dashed curves are for the errors in the three points ($2\Delta x$ error) nearest scale-collapse position. The solid curves exclude the errors in three-point scale-collapse region.

The analytical and second-order finite difference solutions at the time of scale collapse with $N = 32$ and various $\bar{u}$ are illustrated in Fig. 4. The methods and the $\bar{u}$ are as follows: (a) FD2, $\bar{u} = 0.0$; (b) FD2C, $\bar{u} = 0.0$; (c) FD2, $\bar{u} = 0.5$; (d) FD2C, $\bar{u} = 0.5$; (e) FD2, $\bar{u} = 1.0$; (f) FD2C, $\bar{u} = 1.0$. The time step used in the calculation is 0.0078125 ($\ln_2 \Delta t = -7$). Note that FD2 and FD2C yield good results when $\bar{u} = 0$. The solutions degrade somewhat as $\bar{u}$ increases. The root mean square errors in the FD2 and FD2C schemes as a function of $\bar{u}$ for $N = 32$ and $\Delta t = 0.0078125$ ($\ln_2 \Delta t = -7$) are shown in Fig. 5. The dashed curves in Fig. 5 are for the errors in the three points ($2\Delta x$ error) nearest scale-collapse position. The solid curves exclude the errors in three-point scale-collapse region. Figure 5 suggests that as $\bar{u}$ increases errors tend to increase and become less localized in the scale-collapse region. Similar results are obtained with fourth-order finite difference calculations. Thus they are not shown here.

3. Semi-Lagrangian solutions

The simulation of the development of scale-collapse phenomena without the dispersion errors as shown in Fig. 3 is crucial in many areas of atmospheric modeling.

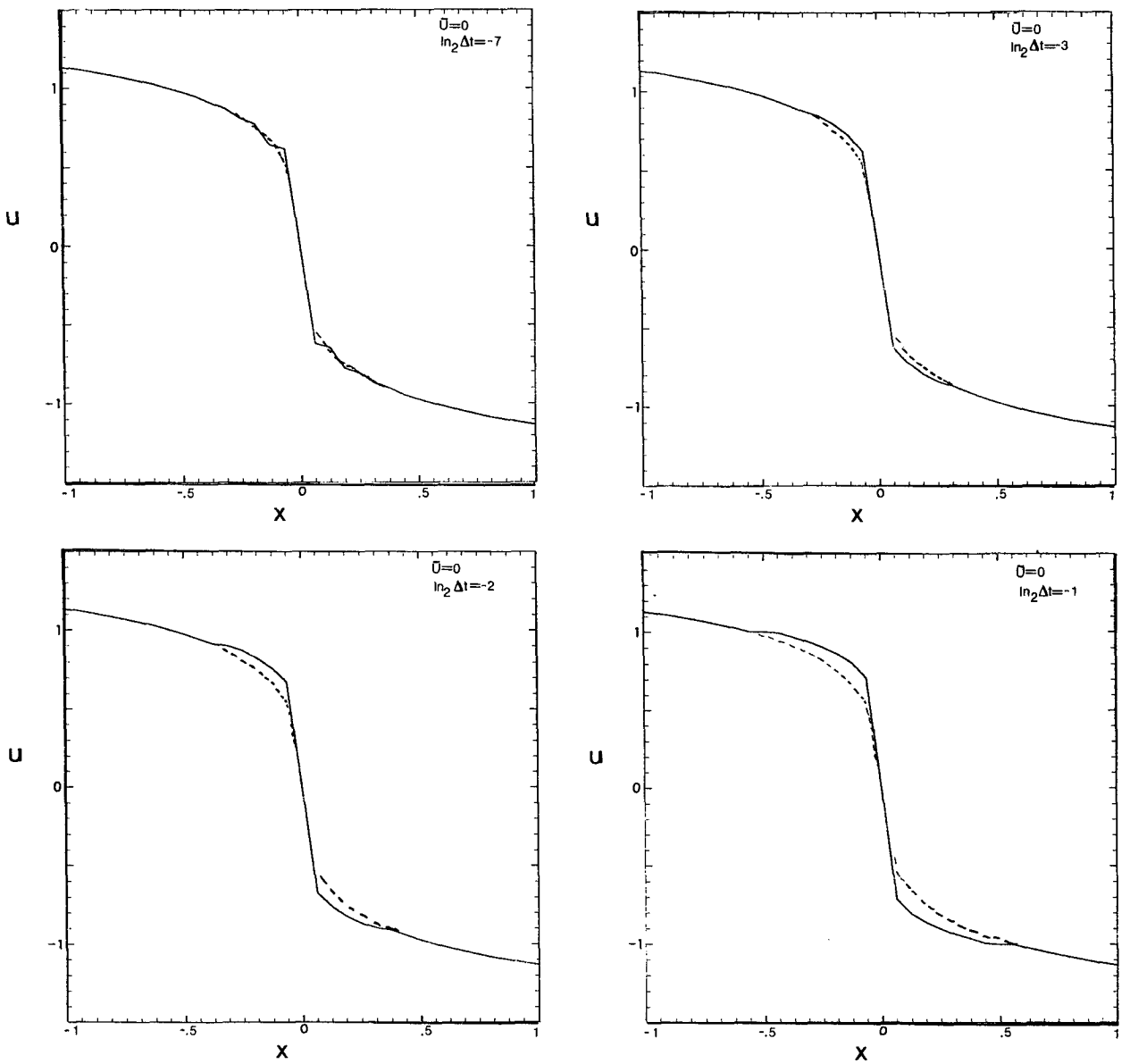

FIG. 6. The analytical and semi-Langrangian solutions at the time of scale-collapse with $N = 32$ and $\bar{u} = 0.0$ and $x_0 = 0.0$. The dashed curves are the analtyical solutions. The time steps are as follows: (a) 0.0078125 ($\ln_2 \Delta t = -7$); (b) 0.125 ($\ln_2 \Delta t = -3$); (c) 0.25 ($\ln_2 \Delta t = -2$); (d) 0.5 ($\ln_2 \Delta t = -1$).

We will now examine the evolution of the scale collapse with the semi-Lagrangian method. Again, the boundary conditions used in the calculations are provided by the analytical solution. In the semi-Lagrangian formulation, Eq. (1) is written in the form of a total derivative following the motion

$$\frac{d}{dt}u(x(t), t) = 0. \tag{7}$$

In a centered scheme it is approximated as

$$\frac{u(x(t + \Delta t), t + \Delta t) - u(x(t - \Delta t), t - \Delta t)}{2\Delta t} = 0. \tag{8}$$

Choosing the location at the forecast time to correspond to a grid point (i.e., $x\ (t + \Delta t) = x_j$), and letting α_j represent the displacement during one time step leads to

$$u(x_j, t + \Delta t) = u(x_j - 2\alpha_j, t - \Delta t). \tag{9}$$

The displacements α_j are determined by approximate integration of

$$\frac{dx}{dt} = u \tag{10}$$

over the period of $[t - \Delta t, t + \Delta t]$. Integration of (10) by the midpoint rule yields

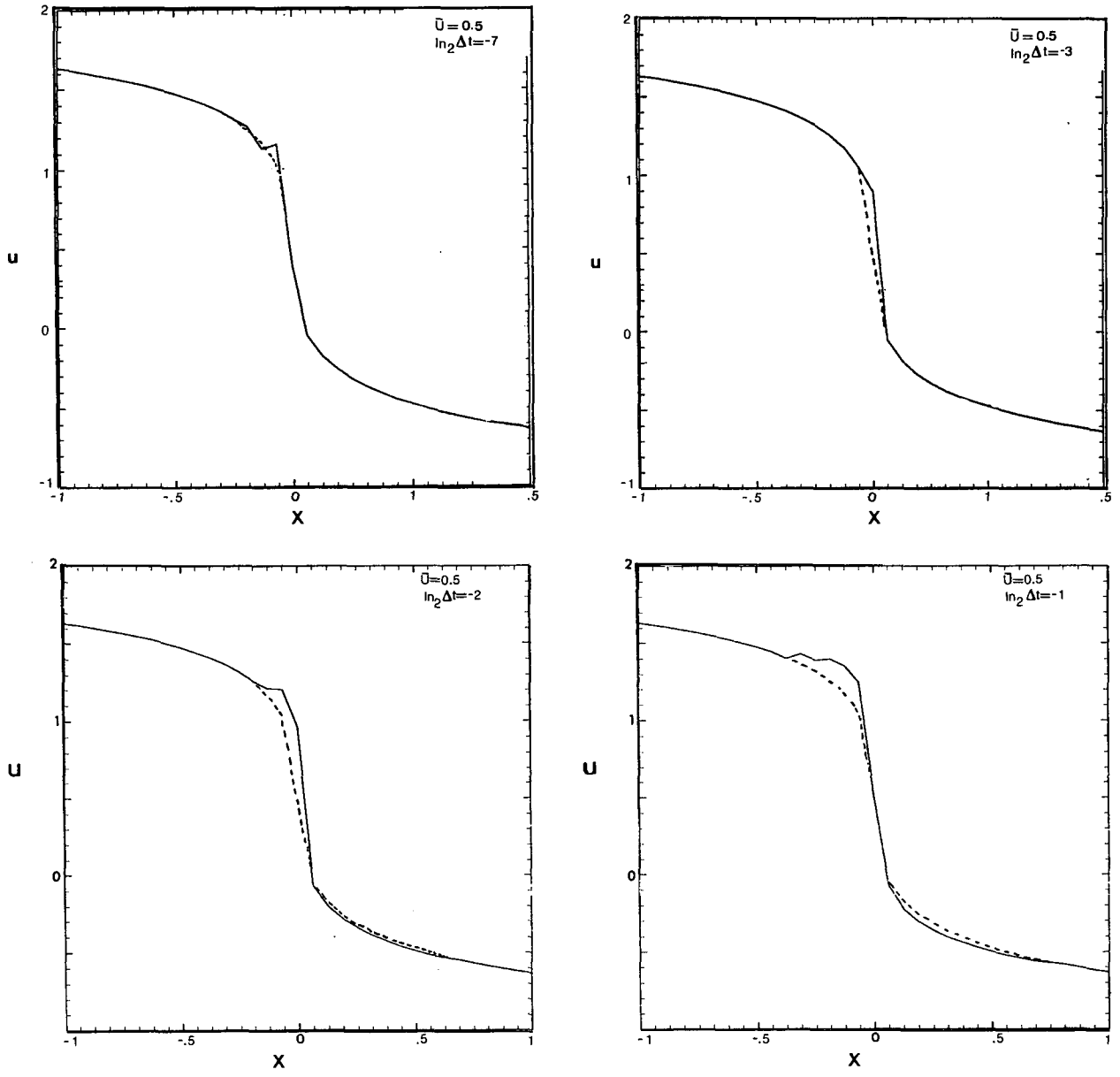

FIG. 7. Same as Fig. 6 except with $\bar{u} = 0.5$ and $x_0 = -0.5$.

$$\alpha_j = \Delta t u(x_j - \alpha_j, t), \tag{11}$$

which can be solved by iteration. The combination of (9) and (11) is the three-time-level semi-Lagrangian scheme with second-order accuracy in time. It is similar to the one proposed by Robert (1981). The assurance of convergence and computational efficiency of iteration will be analyzed by the fixed point iteration, of which many iterative methods (such as Secant and Newton's methods) are special examples (Conte and de Boor 1980). With n fixed point iterations, (11) can be written as

$$\alpha_j^{(n+1)} = \Delta t u(x_j - \alpha_j^{(n)}, t). \tag{12}$$

By subtracting (11) from (12) and using the Lipschitz continuous condition we have

$$\|\alpha_j^{(n+1)} - \alpha_j\| = \Delta t \left\| \frac{\partial u}{\partial x} \right\| \|\alpha_j^{(n)} - \alpha_j\|. \tag{13}$$

From the contraction mapping principle, (13) indicates that iteration in (12) will converge so long as

$$\Delta t \left\| \frac{\partial u}{\partial x} \right\| < 1. \tag{14}$$

Equation (13) also indicates that accuracy is raised by $O(\Delta t)$ with each iteration we perform. Since the midpoint rule used in Eq. (11) is of third-order accuracy

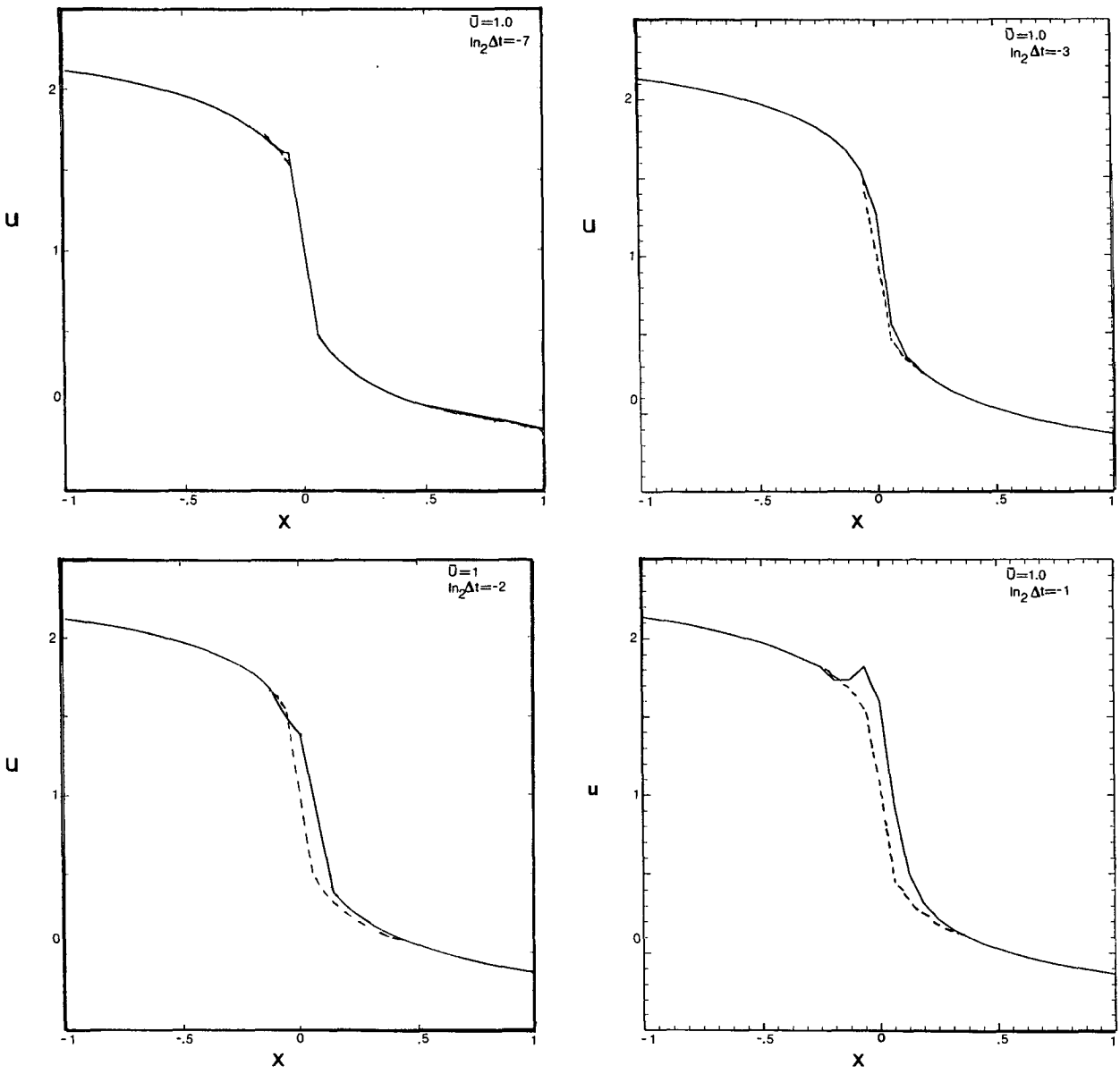

FIG. 8. Same as Fig. 6 except with $\bar{u} = 1.0$ and $x_0 = -1.0$.

in time, no more than three iterations are needed to solve Eq. (11). Condition (14) imposes accuracy constraints on the choice of time-step size used in the semi-Lagrangian method. The time-step size used in the semi-Lagrangian method is limited only by the variation of velocity. This differs from the Eulerian methods where the time-step size is limited by the CFL stability contraint. Similar analysis was presented in Pudykiewicz et al. (1985).

Since interpolation is used in finding function values on each departure point, the semi-Lagrangian method can be easily adapted with irregular grid spacing. To compare with the second-order finite difference results in section 2, we have used constant grid spacing (Δx) in our calculations. The key to the semi-Lagrangian method is the interpolation needed in (9) after the departure points are known from the iterations. For the one-dimensional uniform advection of a passive scalar with linear or parabolic interpolations, the semi-Lagrangian methods are related to first-order upstream or Lax Wendroff schemes (Bates and McDonald 1982). However, the development of the semi-Lagrangian method in the last decade (e.g., Robert 1981; Robert et al. 1985; among others) suggests that linear or parabolic interpolations should not be used in finding the function values (e.g., Eq. (9)]. A common alternative is the third-order accurate cubic spline method. It is global in the sense that the value of the interpolating function at any interpolating point depends on all the given input information. There are local third-order accurate interpolators such as the Hyman method (Hyman 1983) where the value of the interpolating function at any point x depends only on the six given values nearest x. We have tested our problem with the cubic spline and Hyman interpolators and obtained similar results with each. Only the results from the cubic spline interpolator are shown here.

Figure 6 shows the analytical and semi-Lagrangian solutions at the time of scale collapse with $N = 32$ and $\bar{u} = 0.0$ and $x_0 = 0.0$. The time steps are as follows: (a) 0.0078125 ($\ln_2\Delta t = -7$); (b) 0.125 ($\ln_2\Delta t = -3$); (c) 0.25 ($\ln_2\Delta t = -2$); (d) 0.5 ($\ln_2\Delta t = -1$). Similar semi-Lagrangian solutions for $\bar{u} = 0.5$ and $x_0 = -0.5$ and $\bar{u} = 1.0$ and $x_0 = -1.0$ are presented in Figs. 7 and 8, respectively. In these figures, the scale-collapse region develops while it is advected from x_0 to $x = 0.0$. The Courant number is greater than 1 in the $\Delta t = 0.125$ case and is greater than two in the $\Delta t = 0.25$ case. When $\Delta t = 0.5$, the Courant number is greater than 4 and the shock forms from the smooth initial condition in only two time-steps.

It is clear from Figs. 6, 7, and 8 that, except for the $\Delta t = 0.5$ case, the semi-Lagrangian solutions maintain the steep gradients while moving with a mean background advection. Even with the $\Delta t = 0.5$ case, when the shock forms from the smooth initial condition in only two time-steps, the semi-Lagrangian solutions are still reasonable. We do not observe large dispersion errors such as those shown in Fig. 3 associated with the semi-Lagrangian solutions. As $\partial u/\partial x$ approaches infinity at the time of scale collapse, (14) indicates the parcel trajectories as determined from (12) fail to converge. Thus, there are errors in the scale-collapse region in addition to the error in interpolation that become increasingly important as the length scale collapses.

Another remarkable feature of semi-Lagrangian solutions is that the errors are confined near the local region of steepest slope. The errors as a function $\bar{u}$ for $N = 32$ with $\ln_2\Delta t = -2$, -4 and -6 are shown in Fig. 9. The conventions of dashed and solid curves are the same as Fig. 5. By comparing Figs. 9 and 5, we note that error is more localized in semi-Lagrangian solutions for a wide range of $\bar{u}$. Moreover, semi-Lagrangian solutions perform well in the scale-collapse situation even when the Courant number is greater than 2. The errors as a function of the time-step size for $N = 32$ with $\bar{u} = 0.0$, 0.3, 0.5, 0.7 and 1.0 at the time of scale collapse are shown in Fig. 10. The conventions of dashed and solid curves are the same as Fig. 5. Figure 10 reinforces the observation from Figs. 6, 7, and 8 that the semi-Lagrangian solutions agree well with the analytical solution except for the small oscillations around the scale-collapse region. It is highly desirable that the solutions away from the scale-collapse region are not affected by the presence of the scale-collapse region. From Figs. 9 and 10 we note that this is true

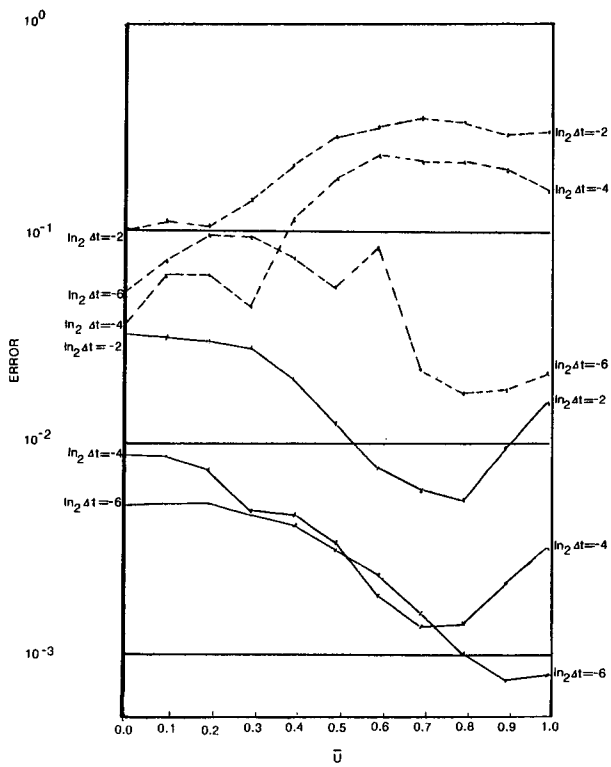

FIG. 9. The root mean square error in semi-Lagrangian method as a function $\bar{u}$ for $N = 32$ and $\ln_2\Delta t = -2$, -4, and -6 at the time of scale collapse. The convention of dashed and solid curves are the same as Fig. 5.

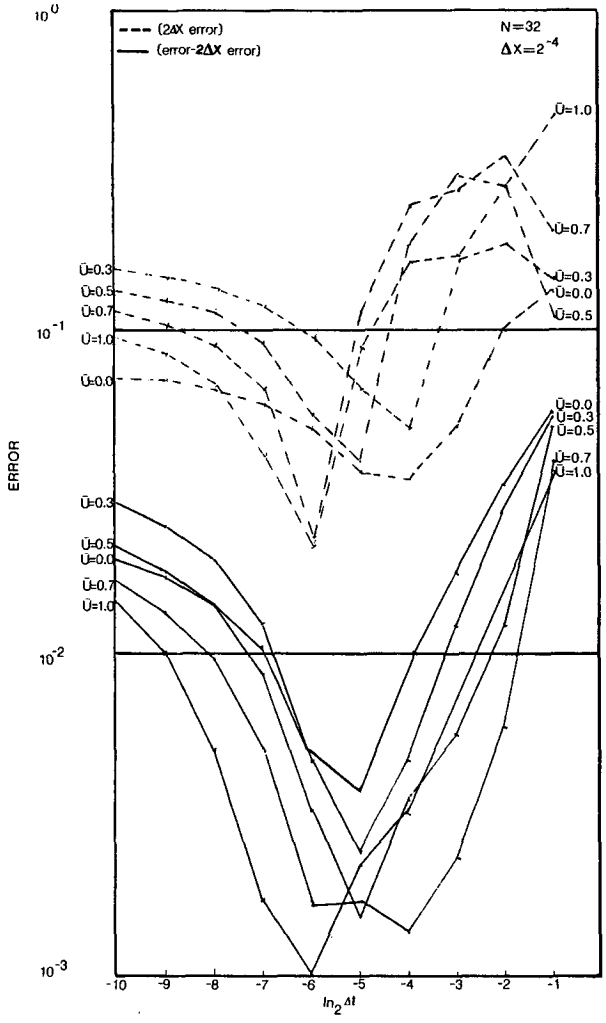

FIG. 10. The root-mean-square error in the semi-Lagrangian solutions of the inviscid Burgers equation as a function of the time-step size (Δt) for $N = 32$ with $\bar{u} = 0.0$, 0.3, 0.5, 0.7 and 1.0 at the time of scale collapse. Dashed and solid curves mean the same as in Fig. 5.

even when the Courant numbers are greater than 4. The properties of localized errors and larger time steps in the semi-Lagrangian method enable us to simulate efficiently the evolution of a steep gradient or near discontinuity in a numerical model.

Finally, we note that the errors in Fig. 10 are "V" shaped with respect to the time-step size. The minima in these "V" shaped curves are associated with the time steps of Courant number approximately equal to 1. On the left part of the "V" shaped curves, the interpolation errors dominate. Thus the accuracy of semi-Lagrangian solutions improves when larger time steps are used (the number of interpolations are reduced). On the right part of the "V" shaped curves where Courant numbers are greater than 1, time truncation errors dominate. Therefore the errors of the semi-Lagrangian solutions increase as the time-step sizes increase. Figure 11 illustrates the error as a function of the number of grid points N for the two different time-step sizes that have errors on both sides of the "V" curves. It is clear that the accuracy improves as N increases when the time step is sufficiently small (Courant number is smaller than 1 and interpolation errors dominate). No improvement of accuracy by increasing N is found in the situation where time truncation errors dominate. This suggests that the accuracy in semi-Lagrangian model can be further improved when time truncation errors are reduced. This may, however, lead to a reduction in efficiency.

4. Concluding remarks

The semi-Lagrangian method has generally been applied to synoptic scale modeling. In those studies the spatial scales of flows did not change appreciably during

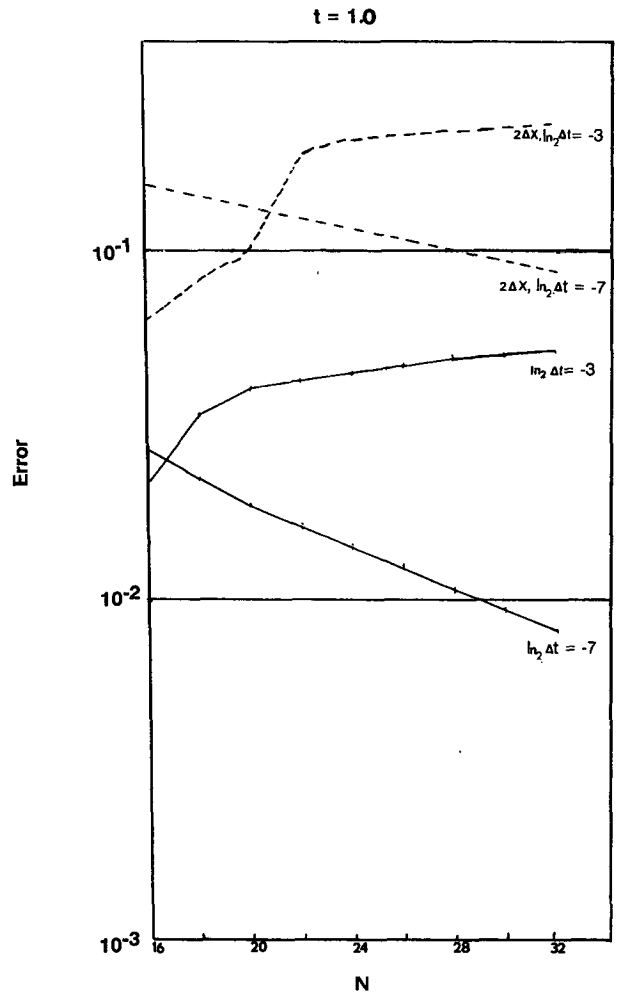

FIG. 11. The root-mean-square error in the semi-Lagrangian solutions of the inviscid Burgers equation as a function of the number of grid points N at scale-collapse time. The time steps are 0.125 ($\ln_2 \Delta t = -3$) and 0.0078125 ($\ln_2 \Delta t = -7$). Dashed and solid curves mean the same as in Fig. 5.

the forecast period. Here we explore the use of semi-Lagrangian methods in the situation where the scale of the flow collapses to zero during the integration. The inviscid Burgers equation is used because of the shock formation in the solution and the existence of analytical solutions. The test model analytical solutions as shown in Fig. 1 resemble the classical case of frontogenesis by deformation fields (Hoskins and Bretherton 1972). Thus we believe the present semi-Lagrangian calculations are representative and related to the atmospheric modeling. Despite the manner in which the gradient of the wind approaches infinity in a portion of domain the semi-Lagrangian schemes perform well with larger time steps (Courant number greater than 2 or 4) than the Eulerian methods. We have shown that the semi-Lagrangian method gives solutions with much less dispersion error at the time of scale collapse. Specifically, most of the errors are localized in the $2\Delta x$ region nearest the shock. The semi-Lagrangian solutions away from the shock are not affected by the presence of the shock. The results indicate the usefulness of the semi-Lagrangian method in handling the advection of near discontinuities and the development of scale-collapse regions in atmospheric numerical models.

Acknowledgments. This work is supported by UCAR Visiting Scientist Program at Naval Environmental Prediction Research Facility with the additional support by the Naval Postgraduate School for the Office of Naval Research. The authors have benefited greatly from the comments of Drs. Gary Dietachmayer, Wayne Schubert and James Toth. The computer calculations were performed at Naval Environmental Prediction Research Facility. The authors would like to thank Ms. A. Gilbert for assistance in the preparation of this paper.

REFERENCES

Bates, J. R., 1984: An efficient semi-Lagrangian and alternating-direction implicit method for integrating the shallow water equations. *Mon. Wea. Rev.*, **112**, 2033–2047.

——, and A. McDonald, 1982: Multiple-upstream, semi-Lagrangian advective schemes: Analysis and application to a multi-level primitive equation model. *Mon. Wea. Rev.*, **110**, 1831–1842.

Bretherton, F. P., 1966: Critical layer instability in baroclinic flows. *Quart. J. Roy. Meteor. Soc.*, **92**, 325–334.

Conte, S. D., and C. de Boor, 1980: *Elementary numerical analysis.* McGraw-Hill, 432 pp.

Cote, J., and A. Staniforth, 1988: A two time-level semi-Lagrangian semi-implicit scheme for spectral models. *Mon. Wea. Rev.*, **116**, 2003–2012.

Gottlieb, D., and S. A. Orszag, 1977: *Numerical Analysis of Spectral Methods: Theory and Applications.* Regional conference series in applied mathematics, No. 26, Society for Industrial and Applied Mathematics, 172 pp.

Hoskins, B. J., and F. P. Bretherton, 1972: Atmospheric frontogenesis models: Mathematical formulation and solution. *J. Atmos. Sci.*, **29**, 11–37.

——, M. E. McIntyre and A. W. Robertson, 1985: On the use and significance of isentropic potential vorticity maps. *Quart. J. Roy. Meteor. Soc.*, **111**, 877–946.

Hyman, J. M., 1983: Accurate monotonicity preserving cubic interpolations. *SIAM J. Sci. Stat. Comput.*, **4**, 645–654.

McDonald, A., 1986: A semi-Lagrangian and semi-implicit two-level integration scheme. *Mon. Wea. Rev.*, **114**, 824–830.

Pudykiewicz, J., and A. Staniforth, 1984: Some properties and comparative performance of the semi-Lagrangian method of Robert in the solution of the advection-diffusion equation. *Atmos. Ocean.*, **22**, 283–308.

——, R. Benoit and A. Staniforth, 1985: Preliminary results from a partial LRTAP model based on an existing meteorological forecast model. *Atmos. Ocean*, **23**, 267–303.

Robert, A. J., 1981: A stable numerical integration scheme for the primitive meteorological equations. *Atmos. Ocean.*, **19**, 35–46.

——, J. Henderson and C. Turnbull, 1972: An implicit time integration scheme for baroclinic models of the atmosphere. *Mon. Wea. Rev.*, **100**, 329–335.

——, T. L. Yee and H. Ritchie, 1985: A semi-Lagrangian and semi-implicit numerical integration scheme for multi-level atmospheric models. *Mon. Wea. Rev.*, **113**, 388–394.

Sawyer, J. S., 1963: A semi-Lagrangian method of solving the vorticity advection equation. *Tellus*, **15**, 336–342.

Shapiro, M. A., T. Hampel, D. Rotzoll and F. Mosher, 1985: The frontal hydraulic head: The micro γ scale (1 km) triggering mechanism for mesoconvective weather systems. *Mon. Wea. Rev.*, **113**, 1166–1183.

Smolarkiewicz, P. K., 1984: A fully multidimensional positive definite advection transport algorithm with small implicit diffusion. *J. Comput. Phys.*, **54**, 325–362.

Staniforth, A., and C. Temperton, 1986: Semi-implicit semi-Lagrangian integration schemes for a barotropic finite-element regional model. *Mon. Wea. Rev.*, **114**, 2078–2090.

Takacs, L. L., 1985: A two-step scheme for the advection equation with minimized dissipation and dispersion errors. *Mon. Wea. Rev.*, **113**, 1050–1065.

Tanguay, M., A. Simard and A. Staniforth, 1989: A three-dimensional semi-Lagrangian scheme for Canadian regional finite-element forecast model. *Mon. Wea. Rev.*, **117**, 1861–1871.

Temperton, C., and A. Staniforth, 1987: An efficient two-time level semi-Lagrangian semi-implicit integration scheme. *Quart. J. Roy. Meteor. Soc.*, **113**, 1025–1039.

Whitham, G. B., 1974: *Linear and Nonlinear Waves.* John Wiley, 636 pp.

Wiin-Nielsen, A., 1959: On the application of trajectory methods in numerical forecasting. *Tellus*, 11, 180–196.

Williams, R. T., 1967: Atmospheric frontogenesis: A numerical experiment. *J. Atmos. Sci.*, **24**, 627–641.

——, 1972: Quasi-geostrophic versus non-geostrophic frontogenesis. *J. Atmos. Sci.*, **29**, 3–10.

——, and R. P. Kurth, 1976: Formation of discontinuities in a stratified rotating atmosphere. *J. Geophys. Res.*, **81**, 1133–1140.

Williamson, L. D., and P. J. Rasch, 1989: Two-dimensional semi-Lagrangian transport with shape-preserving interpolation. *Mon. Wea. Rev.*, **117**, 102–129.

Woodward, P. R., and P. Colella, 1984: The numerical simulation of two-dimensional fluid flow with strong shocks. *J. Comput. Phys.*, **54**, 115–123.